© 2016 IEEE. Personal use of this material is permitted. Permission from IEEE must be obtained for all other uses, in any current or future media, including reprinting/republishing this material for advertising or promotional purposes, creating new collective works, for resale or redistribution to servers or lists, or reuse of any copyrighted component of this work in other works.

J. Iannacci; M. Huhn; C. Tschoban; H. Pötter, **RF-MEMS Technology for Future Mobile and High-Frequency Applications: Reconfigurable 8-Bit Power Attenuator Tested up to 110 GHz**, IEEE ELECTRON DEVICE LETTERS, Volume: 37, Issue: 12, Dec. 2016, pp. 1646 – 1649, DOI: 10.1109/LED.2016.2623328

The final published version is available online at: https://ieeexplore.ieee.org/document/7726036

When citing, please refer to the published version.

Copyright (c) 2016 IEEE. Personal use is permitted. For any other purposes, permission must be obtained from the IEEE by emailing pubs-permissions@ieee.org.

RF-MEMS Technology for Future Mobile and High-Frequency Applications: Reconfigurable 8-Bit Power Attenuator Tested up to 110 GHz

J. Iannacci, M. Huhn, C. Tschoban, and H. Pötter

Abstract—**In this work, we present and test – to the best of our knowledge, for the first time –, an 8-bit (256-state) reconfigurable RF-MEMS attenuator, from 10 MHz up to 110 GHz, realized in the CMM-FBK technology. Resistive loads, in series and shunt configuration, are selectively inserted on the RF line by means of electrostatic MEMS ohmic switches. The network exhibits several attenuation levels in the range of -10/-45 dB that are rather flat up to 50 GHz, and a certain number of configurations with VSWR smaller than 4 from nearly-DC up to 110 GHz, and better than 2 on a frequency span of about 80 GHz.**

Index Terms—**RF-MEMS, reconfigurable attenuators, tunable passives, 5G applications, wideband operability, S-parameters, low-loss, FEM modeling, 110 GHz.**

I. Introduction

THE remarkable characteristics of RF-MEMS passives, i.e. MicroElectroMechanical-Systems for Radio Frequency applications, were demonstrated and are well-known since the late '90s [1]. The superior performance figures in terms of low-loss, high-isolation, high Q-factor, linearity of switches (ohmic/capacitive), varactors, inductors, resonators, LC-tanks in RF-MEMS technology were stared as a landmark for modern radio and RF systems [2,3]. In fact, the large market uptake of RF-MEMS, forecasted in the first years of 2000, never took place. All in all, if on one hand reliability [4] and packaging/integration [5] were still open issues, on the other side, early generations of mobile devices were not demanding for the boosted performance of MEMS-based passives [6].

More recently, RF-MEMS components commenced to be adopted in 4G-LTE smartphones to improve the quality of voice and data transmission (i.e. market-driven context) [7].

From a different perspective, 5G systems will demand for higher operation frequencies and large reconfigurability to cover different services, while reducing hardware redundancy and power consumption [8]. Scoring such targets means leveraging on passives with boosted features, and RF-MEMS technology could be a viable solution, both for 5G RF Front Ends (RFFEs) and base stations [9].

In this work, we test and simulate (Finite Element Method – FEM analysis) an 8-bit (256-state) reconfigurable RF-MEMS power attenuator up to 110 GHz. Resistive loads, in series and shunt configuration, are selectively inserted on the RF line, depending on the state (ON/OFF) of electrostatic MEMS ohmic switches. The network shows attenuation levels in the range of -10/-45 dB with pronounced flatness up to 50 GHz. Margins of improvement at design level are also discussed.

Second revised version submitted for final review October 27, 2016.

J. Iannacci is with Fondazione Bruno Kessler (FBK), Trento, 38123 Italy (e-mail: iannacci@fbk.eu).

M. Huhn, C. Tschoban, and H. Pötter are with the Fraunhofer Institut für Zuverlässigkeit und Mikrointegration IZM, Berlin, 13355 Germany (e-mail: max.huhn@izm.fraunhofer.de; christian.tschoban@izm.fraunhofer.de; harald.poetter@izm.fraunhofer.de).

II. RF-MEMS 8-Bit Reconfigurable Power Attenuator

The reconfigurable 8-bit power attenuator is realized in the RF-MEMS surface micromachining process available at the Center for Materials and Microsystems (CMM) of Fondazione Bruno Kessler (FBK), in Italy. It features 9 lithographic steps and 2 buried conductive layers: doped polycrystalline Silicon (poly-Si) and multi-metal stack based on Aluminum [10,11].

The photograph of an RF-MEMS attenuator sample and the equivalent lumped-element schematic are shown in Fig. 1.

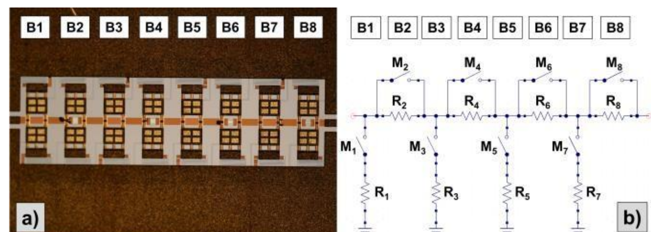

Fig. 1. a) Photograph of an RF-MEMS attenuator physical sample. Eight cascaded switching units are visible and labelled as B1 to B8. The whole network dimensions are 3 mm by 1.95 mm. b) Equivalent (ideal) schematic of the attenuator. Four shunt-to-RF ground resistors ($R_{1,3,5,7}$) are alternated to four series loads ($R_{2,4,6,8}$). They are selected/deselected by means of 8 independently controlled electrostatic MEMS ohmic switches (M1 to M8).

Standalone 1-bit basic attenuator modules were reported in [12]. The network in Fig. 1a features 8 cascaded bits (B1 to B8) that exploit poly-Si (140 Ω/sq) resistors in shunt-to-RF ground ($R_{1,3,5,7}$ in Fig. 1b) and series configuration ($R_{2,4,6,8}$ in Fig. 1b) to attenuate the signal, and 8 MEMS ohmic switches (M_{1-8} in Fig. 1b) to select or deselect/short them. Details on the network and electrical parameters are reported in Table I.

TABLE I
Electrical Parameters of the RF-MEMS Network in Fig. 1.

Bit	Load	Loading the RF line when
B1	$R_1 \approx 0\ \Omega$ (shunt)	M_1 is ON (B1 state = 1)
B2	$R_2 = 140\ \Omega$ (series)	M_2 is OFF (B2 state = 0)
B3	$R_3 = 42\ \Omega$ (shunt)	M_3 is ON (B3 state = 1)
B4	$R_4 = 174\ \Omega$ (series)	M_4 is OFF (B4 state = 0)
B5	$R_5 = 42\ \Omega$ (shunt)	M_5 is ON (B5 state = 1)
B6	$R_6 = 256\ \Omega$ (series)	M_6 is OFF (B6 state = 0)
B7	$R_7 = 42\ \Omega$ (shunt)	M_7 is ON (B7 state = 1)
B8	$R_8 = 575\ \Omega$ (series)	M_8 is OFF (B8 state = 0)

Copyright (c) 2016 IEEE. Personal use is permitted. For any other purposes, permission must be obtained from the IEEE by emailing pubs-permissions@ieee.org.

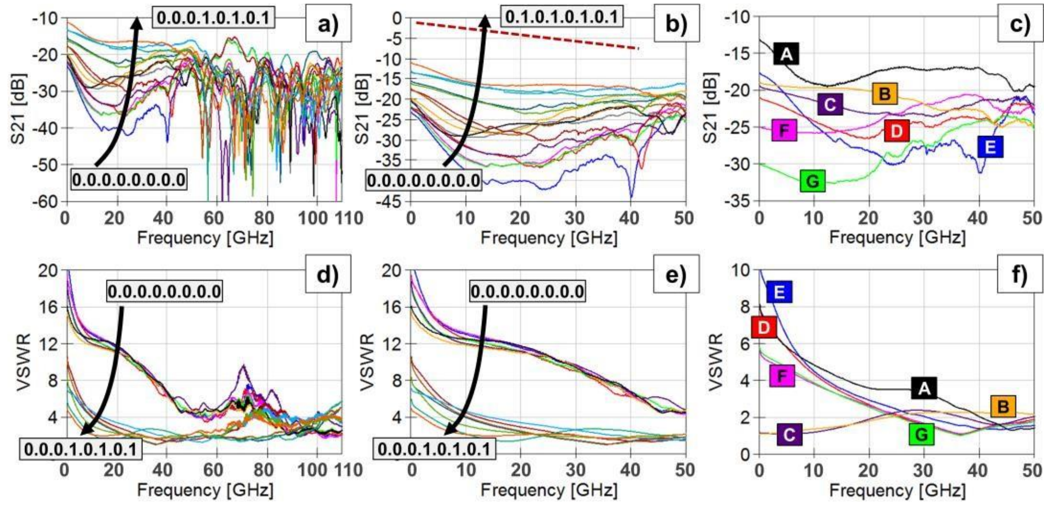

Fig. 2. Measured attenuation (S21 parameter) (a-b) and Voltage Standing Wave Ratio (VSWR) (d-e) of the RF-MEMS network in Fig. 1, from 10 MHz to 110 GHz – (a) and (d), respectively – and from 10 MHz to 50 GHz – (b) and (e), respectively – for configurations with/without series resistances (15 different traces), i.e. B1.B8 from 0.0.0.0.0.0.0.0 to 0.0.0.1.0.1.0.1 (see Fig. 1 and Table I). Measured S21 (c) and VSWR (f) from 10 MHz to 50 GHz for configurations also involving shunt sections. The labels are as follows: A = 0.0.0.1.0.1.0.1; B = 0.0.0.0.0.1.1.1; C = 0.0.0.0.1.1.0.1; D = 0.1.1.0.0.0.0.1; E = 0.0.0.0.0.0.0.1; F = 0.0.1.1.0.0.0.1; G = 0.0.0.1.1.0.0.1. More discussion on the dashed line in (b) (i.e. OFF attenuator configuration) is developed in the text and in Fig. 3.

The device is framed within a Coplanar Waveguide (CPW) structure, designed to match 50 Ω characteristic impedance.

III. Experimental Testing and FEM Simulations

S-parameters are tested on-wafer with a Programmable Network Analyzer (PNA) and Ground Signal Ground (GSG) probes, separately calibrated with Line-Reflect-Reflect-Match (LRRM) method (0 dBm power; 50 Ω impedance) in the 10 MHz to 67 GHz and 67 to 110 GHz ranges, to achieve better accuracy [12].

In this letter, we focus on the 4 series resistive loads (B2,4,6,8 in Fig. 1 and Table I) and on few configurations involving shunt sections (B1,3,5,7). Fig. 2 reports the measured attenuation (S21) (Fig. 2a-b) and the Voltage Standing Wave Ratio (VSWR) (Fig. 2d-e) for the 15 configurations ranging from larger to smaller series resistance, i.e. B1.B8 from 0.0.0.0.0.0.0.0 to 0.0.0.1.0.1.0.1 (see Table I). For completeness, we report the whole measured range from 10 MHz to 110 GHz (Fig. 2a,d) and a focused range up to 50 GHz (Fig. 2b,e). For shunt configurations, we focus for brevity on the range from 10 MHz to 50 GHz (Fig. 2c,f).

The network shows attenuation (S21) levels in the range of -10/-45 dB from 10 MHz to 110 GHz (Fig. 2a). They exhibit a flatness over frequency of about 15 dB in the worst case (larger resistance), to values as small as 5-6 dB for the configurations with lower series resistance, in the sub-range up to 50 GHz (Fig. 2b). A clear dependence of the attenuation on the amount of resistance loading the RF line is visible.

Important indications on the device behavior come from the VSWR. Looking only at the S21 is misleading, as high attenuations can appear also when most part of the signal is reflected at the input port (i.e. large S11) due to severe impedance mismatch. For this reason, we consider in this discussion as reasonable threshold for the VSWR the value of 4. Below such a limit, the reflected power is smaller than 36 % and, therefore, the corresponding attenuation is mainly due to the RF signal travelling across the RF-MEMS network.

In light of these considerations, when looking at the VSWR in Fig. 2d-e, only about half of the analyzed configurations can be regarded as exploitable to effectively attenuate RF signals (i.e. VSWR below 4), and correspond to the network configurations with smaller series resistance. However, it must be kept in mind that all the resistive loads in Table I are oversized with respect to design. The measured vs. nominal poly-Si resistance value is 140 Ω/sq instead of 100 Ω/sq [12]. Moreover, wide margins to modify the form factor of resistors and reduce, in turn, their load, are viable at design level.

Attenuation levels from 50 to 110 GHz (Fig. 2a,d) exhibit a more complex behavior and much less pronounced flatness. However, most part of them show a VSWR well-below 4 across the whole span. The non-linear S21 characteristics in Fig. 2c-d can be significantly mitigated by redesigning the network in Fig. 1 and the MEMS switches, in order to be more compact, thus reducing parasitic effects [12].

Further insight of the network behavior is provided by the hybrid configurations, involving both series and shunt modules, reported in Fig. 2c,f. As visible in Fig. 2c, the attenuation spans in the same range reported in Fig. 2b. Nonetheless, interesting indications emerge from the VSWR in Fig. 2e. Let us take as reference the configuration A = 0.0.0.1.0.1.0.1, where 3 out of 4 series resistances are shorted and no shunt paths are activated, and let us compare it to B = 0.0.0.0.0.1.1.1 and C = 0.0.0.0.1.1.0.1, where the total series resistance is lower than in case A and a shunt module is also activated. Despite the A state shows the lowest attenuation (-12/-20 dB), its VSWR is definitely worse than B and C, up to around 40 GHz (Fig. 2f), the latter ones presenting a VSWR better than 2.4 from 10 MHz to 50 GHz. Moreover, looking at the traces B, C, D, F, G, rather flat attenuation characteristics in the range of -20/-33 dB are achieved, keeping the VSWR always below 4, from 10 GHz and rising. This means that, as long as series resistors are decreased, better performance will be achieved in improved attenuator redesign, just combining series and shunt loads.

Copyright (c) 2016 IEEE. Personal use is permitted. For any other purposes, permission must be obtained from the IEEE by emailing pubs-permissions@ieee.org.

We also measured the configuration with all the resistors shorted (0.1.0.1.0.1.0.1), using 4 DC probes at the same time. Due to the limited current compliance of the available DC voltage source, MEMS switches were self-releasing during measurements. Despite that, we managed to observe a rather linear and limited loss (S21) in the range -1/-7 dB up to 40 GHz, shown in Fig. 3, and reported in Fig. 2b (dashed line) for comparison with the other configurations.

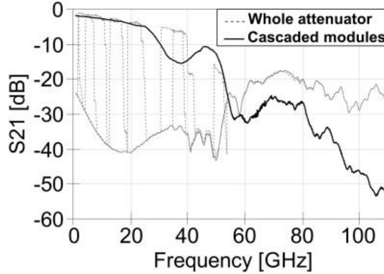

Fig. 3. Measured loss (S21) for B1.B8 = 0.1.0.1.0.1.0.1 (dashed lines). The repeated switches' releases (vertical transitions) are visible. The solid line is obtained by cascading the measured S-parameter datasets of the series and shunt basic attenuator modules, reported in [12].

In order to get precise indications of the typical network loss when OFF, we built a schematic within the Quite Universal Circuit Simulator (QUCS – qucs.sourceforge.net), not shown here for brevity. We cascaded S-parameters measured datasets (Touchstone format) of the basic shunt and series attenuator modules, already reported in [12], in the OFF state (for B1,3,5,7) and ON state (for B2,4,6,8), respectively, thus miming the 0.1.0.1.0.1.0.1 configuration of the network in Fig. 1. The result is reported in Fig. 3 (solid line) and well-compares to the measurements of the whole network (dashed lines) up to around 60 GHz. It must be kept in mind that cascading 8 basic modules leads, in terms of loss (S21), to a case worse than the whole network. In the former layouts, indeed, there are more vertical layer transitions between the Aluminum buried layer and the Gold metallizations [11-12], not present in the latter device. This brings in additional series parasitic resistance worsening the S21, especially above 60 GHz. Though, the rationale beneath cascading 8 single modules is to prove that the partial results of the whole network (dashed lines in Fig. 3) are consistent.

Eventually, we built a 3D model of the RF-MEMS network in Fig. 1 and performed FEM simulations in Ansys HFSS. Fig. 4 shows the close-up of the B2 switch in HFSS.

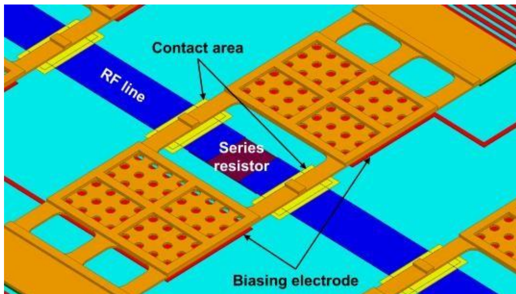

Fig. 4. Close-up of the HFSS 3D model, showing the B2 switch (see Fig. 1). The buried series resistor, contact areas for shorting the load (when the switch is pulled-in), the RF line and DC biasing electrodes, are highlighted.

The vertical quote of each MEMS switch is parameterized to easily reconfigure the attenuator state. The micro-relays are clamped-clamped electrostatically controlled devices, it being one of the most robust design solutions, in terms of mechanical reliability and cycling, realized in the CMM-FBK RF-MEMS technology [13-14]. Prior to RF testing, we characterized the DC behavior of the switches, observing a rather stable and repeatable actuation (pull-in) of the MEMS micro-relays, in the range of 45/50 V. We did not encounter any stiction condition (i.e. missed release of the switch when the DC bias is zeroed [15]), possibly induced by charge injection and/or micro-welding, in all of the tested samples.

Fig. 5 shows the measured vs. simulated attenuation (S21) and reflection (S22) in a few different configurations.

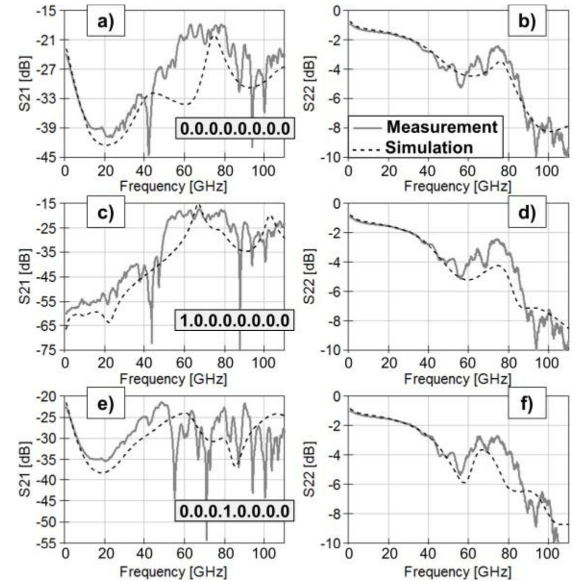

Fig. 5. Comparison of the measured vs. simulated (HFSS) attenuation (S21) and reflection (S22) for the following network configurations (see Fig. 1 and Table I): 1) 0.0.0.0.0.0.0.0 – S21 (a), S22 (b); 2) 1.0.0.0.0.0.0.0 – S21 (c), S22 (d); 3) 0.0.0.1.0.0.0.0 – S21 (e), S22 (f).

The HFSS predicts the S-parameters with good accuracy up to 110 GHz, in all the studied configurations. The 3D model in Fig. 4 will be an important tool in redesigning the discussed RF-MEMS concept and optimize its characteristics, according to the considerations previously developed in this work.

IV. Conclusions

In this letter, we presented, tested and discussed – to the best of our knowledge, for the first time – an 8-bit (256-state) reconfigurable RF power attenuator fabricated in RF-MEMS technology, in the frequency range from 10 MHz to 110 GHz.

Our concept, manufactured in the RF-MEMS technology available at Fondazione Bruno Kessler (CMM-FBK), in Italy, features 8 resistive loads, 4 in series and 4 in shunt configuration, that are selectively inserted on the RF line by means of 8 electrostatic independent MEMS ohmic switches. The whole network footprint is of just 3 mm by 1.95 mm.

We measured attenuations (S21) in the range of -10/-45 dB with flatness as good as 5-6 dB up to 50 GHz, and VSWR below 4. 3D FEM simulations were also reported and validated against experiments. The shown accurate predictive model will be the basis to implement several improvements at design optimization level, also discussed in this work.

Copyright (c) 2016 IEEE. Personal use is permitted. For any other purposes, permission must be obtained from the IEEE by emailing pubs-permissions@ieee.org.

REFERENCES

[1] G. M. Rebeiz, *RF MEMS: Theory, Design, and Technology*, 1st ed. Hoboken, NJ; John Wiley & Sons, 2003, pp. 1–512.

[2] A. Kaiser, “The potential of MEMS components for re-configurable RF interfaces in mobile communication terminals,” in *Proc. ESSCIRC*, Villach, Austria, 2001, pp. 25–28.

[3] C. T.-C. Nguyen, “Microelectromechanical devices for wireless communications,” in *Proc. IEEE MEMS*, Heidelberg, Germany, 1998, pp. 1–7. DOI: 10.1109/MEMSYS.1998.659719.

[4] J. Iannacci, “Reliability of MEMS: A perspective on failure mechanisms, improvement solutions and best practices at development level,” *Elsevier Displays*, vol. 37, no. xx, pp. 62–71, Apr. 2015. DOI: 10.1016/j.displa.2014.08.003.

[5] J. Iannacci, *Practical Guide to RF-MEMS*, 1st ed. Weinheim, Germany, 2013; Wiley-VCH, 2013, pp. 1–372.

[6] J. Iannacci, “RF-MEMS: an enabling technology for modern wireless systems bearing a market potential still not fully displayed,” *Springer Microsystem Technologies*, vol. 21, no. 10, pp. 2039–2052, Sep. 2015. DOI: 10.1007/s00542-015-2665-6.

[7] Cavendish Kinetics, Inc., “Nubia adopts Cavendish Kinetics' SmarTune Antenna Tuning Solution for its new Z7 LTE Smartphone,” Available online [Accessed 13 October 2016]: http://www.cavendish-kinetics.com/news/news-releases/.

[8] A. Osseiran, F. Boccardi, V. Braun, K. Kusume, P. Marsch, M. Maternia, O. Queseth, M. Schellmann, H. Schotten, H. Taoka, H. Tullberg, M. A. Uusitalo, B. Timus, M. Fallgren, “Scenarios for 5G mobile and wireless communications: the vision of the METIS project,” *IEEE Communications Magazine*, vol. 52, no. 5, pp. 26–35, May 2014.

[9] M. Lapedus, “Inside The 5G Smartphone,” Available online [Accessed 13 October 2016]: http://semiengineering.com/inside-the-5g-smartphone/.

[10] J. Iannacci, F. Giacomozzi, S. Colpo, B. Margesin and M. Bartek, “A General Purpose Reconfigurable MEMS-Based Attenuator for Radio Frequency and Microwave Applications,” in *Proc. IEEE Region 8 EUROCON*, Saint Petersburg, Russia, 2009, pp. 1201–1209. DOI: 10.1109/EURCON.2009.5167788.

[11] F. Giacomozzi, V. Mulloni, S. Colpo, J. Iannacci, B. Margesin and A. Faes, “A Flexible Fabrication Process for RF MEMS Devices,” *Romanian Journal of Information Science and Technology (ROMJIST)*, vol. 14, no. 3, pp. 259–268, 2011. DOI: 10.1109/SMICND.2011.6095744.

[12] J. Iannacci, M. Huhn, C. Tschoban and H. Potter, “RF-MEMS Technology for 5G: Series and Shunt Attenuator Modules Demonstrated up to 110 GHz,” *IEEE Electron Device Letters*, vol. 37, no. 10, pp. 1336–1339, Oct. 2016. DOI: 10.1109/LED.2016.2604426.

[13] J. Iannacci, R. Gaddi, A. Gnudi, “Experimental Validation of Mixed Electromechanical and Electromagnetic Modeling of RF-MEMS Devices Within a Standard IC Simulation Environment,” *IEEE Journal of Microelectromechanical Systems*, vol. 19, no. 3, pp. 526–537, Jun. 2010. DOI: 10.1109/JMEMS.2010.2048417.

[14] J. Iannacci, G. Resta, P. Farinelli, R. Sorrentino, “RF-MEMS Components and Networks for High-Performance Reconfigurable Telecommunication and Wireless Systems,” *Trans Tech Advances in Science and Technology*, vol. 81, no. xx, pp. 65–74, Sep. 2012. DOI: 10.4028/www.scientific.net/AST.81.65.

[15] J. Iannacci, A. Faes, A. Repchankova, A. Tazzoli, G. Meneghesso, “An active heat-based restoring mechanism for improving the reliability of RF-MEMS switches,” *Elsevier Microelectronics Reliability*, vol. 51, no. 9–11, pp. 1869–1873, Sep.–Nov. 2011. DOI: 10.1016/j.microrel.2011.06.019.

Copyright (c) 2016 IEEE. Personal use is permitted. For any other purposes, permission must be obtained from the IEEE by emailing pubs-permissions@ieee.org.